# Evaluating the use of an Unmanned Aerial Vehicle (UAV)-based active AirCore system to quantify methane emissions from dairy cows

Vinković, Katarina; Andersen, Truls; de Vries, Marcel; Kers, Bert; van Heuven, Steven; Peters, Wouter; Hensen, Arjan; van den Bulk, Pim; Chen, Huilin

*Published in:*
The Science of the Total Environment

*DOI:*
10.1016/j.scitotenv.2022.154898



*Publication date:*
2022

Science of the Total Environment 831 (2022) 154898

Contents lists available at ScienceDirect

Science of the Total Environment

journal homepage: www.elsevier.com/locate/scitotenv

# Evaluating the use of an Unmanned Aerial Vehicle (UAV)-based active AirCore system to quantify methane emissions from dairy cows

Katarina Vinković [a], Truls Andersen [a], Marcel de Vries [a], Bert Kers [a], Steven van Heuven [a], Wouter Peters [a,c], Arjan Hensen [d], Pim van den Bulk [d], Huilin Chen [a,b,*]

[a] Centre for Isotope Research (CIO), Energy and Sustainability Research Institute Groningen (ESRIG), University of Groningen, Groningen, the Netherlands
[b] Joint International Research Laboratory of Atmospheric and Earth System Sciences, School of Atmospheric Sciences, Nanjing University, Nanjing, China
[c] Meteorology and Air Quality, Wageningen University and Research Center, the Netherlands
[d] The Netherlands Organisation for Applied Scientific Research (TNO), Circular Economy and Environment Unit, the Netherlands

## HIGHLIGHTS

- UAV-based measurements sufficiently accurate to quantify farm-scale $CH_4$ plumes
- Enteric emission factors of 0.20–0.51 $kgCH_4/AU/day$ (1 AU = 500 kg animal weight)
- UAV provides an effective tool to quantify $CH_4$ emissions from dairy farms.

## GRAPHICAL ABSTRACT


## ARTICLE INFO

Editor: Anastasia Paschalidou

*Keywords:*
Methane
Enteric EFs
UAV
AirCore
Dairy farm

## ABSTRACT

Enteric fermentation and manure methane emissions from livestock are major anthropogenic greenhouse gas emissions. In general, direct measurements of farm-scale methane emissions are scarce due to the source complexity and the limitations of existing atmospheric sampling methods. Using an innovative UAV-based active AirCore system, we have performed accurate atmospheric measurements of $CH_4$ mole fractions downwind of a dairy cow farm in the Netherlands on four individual days during the period from March 2017 to March 2019. The total $CH_4$ emission rates from the farm were determined using the UAV-based mass balance approach to be 1.1–2.4 g/s. After subtracting estimated emission factors of manure onsite, we derived the enteric emission factors to be 0.20–0.51 $kgCH_4/AU/d$ (1 AU = 500 kg animal weight) of dairy cows. We show that the uncertainties of the estimates were dominated by the variabilities in the wind speed and the angle between the wind and the flight transect. Furthermore, nonsimultaneous sampling in the vertical direction of the plume is one of the main limiting factors to achieving accurate estimate of the $CH_4$ emissions from the farm. In addition, a $N_2O$ tracer release experiment at the farm was performed when both a UAV and a mobile van were present to simultaneously sample the $N_2O$ tracer and the $CH_4$ plumes from the farm, improving the source quantification with a correction factor of 1.04 and 1.22 for the inverse Gaussian approach and for the mass balance approach, respectively. The UAV-based active AirCore system is capable of providing useful estimates of $CH_4$ emissions from dairy cow farms. The uncertainties of the estimates can be improved when combined with accurate measurements of local wind speed and direction or when combined with a tracer approach.

* Corresponding author at: Centre for Isotope Research (CIO), Energy and Sustainability Research Institute Groningen (ESRIG), University of Groningen, Groningen, the Netherlands.
*E-mail address:* Huilin.Chen@rug.nl (H. Chen).

http://dx.doi.org/10.1016/j.scitotenv.2022.154898
Received 6 November 2021; Received in revised form 4 March 2022; Accepted 25 March 2022
Available online 29 March 2022

## 1. Introduction

Anthropogenic greenhouse gas (GHG) emissions since 1750s have caused a large increase in atmospheric abundance of carbon dioxide ($CO_2$), methane ($CH_4$), and nitrous oxide ($N_2O$), along with economic and population growth (IPCC, 2014). The atmospheric $CH_4$ mole fraction has increased by a factor of ~2.5, from 722 parts per billion (ppb) in pre-industrial times to 1877 ppb in 2019 (WMO GHG Bulletin 2020). During the period 2014–2017, the atmospheric $CH_4$ mole fraction grew 7–12.7 ppb per year, rates that were not observed since the 1980s (Nisbet et al., 2019). $CH_4$ is the second most important anthropogenic greenhouse gas after $CO_2$ in terms of radiative forcing, with a global warming potential of 28 times that of $CO_2$ over a period of 100 years, and a relatively short atmospheric lifetime (~12 years) (Myhre et al., 2013). It is therefore effective to reduce $CH_4$ emissions to mitigate climate warming. To mitigate $CH_4$ emissions, it is crucial to understand the magnitude of $CH_4$ emissions from various sources. In 2017, the agricultural $CH_4$ emissions in the Netherlands accounted for ~6.5% (both enteric fermentation (~4.5%) and manure (~2%)) of the total GHG emissions (Ruyssenaars et al., 2019). However, these emissions are reported based on inventory studies, and lack independent verification with atmospheric measurements.

Methane is emitted to the atmosphere by both natural sources (wetlands, fresh waters, termites, and oceans, etc.) and anthropogenic sources (enteric fermentation and manure, landfills and waste, fossil fuels, biomass burning, etc.). The sources can also be sorted by emitting processes, i.e., biogenic, thermogenic, and pyrogenic (Saunois et al., 2016). In the case of biogenic sources, $CH_4$ is formed during the decomposition of organic matter under conditions where little to no oxygen is available, a.k.a. anaerobic conditions. Among other biogenic sources, $CH_4$ is a by-product of ruminant's digestive process, and the majority of $CH_4$ produced is emitted through the mouth of multi-stomached ruminants (~87%), while a small quantity produced in the intestines is transmitted through the rectum as intestinal gas (~13%) (Saunois et al., 2016). On a global scale, livestock emissions (enteric fermentation and manure) represented one-third of total human-induced emissions for the 2003–2012 period, making it one of the largest sources of $CH_4$ (Saunois et al., 2016).

$CH_4$ emissions from a group of animals (e.g., at a farm scale) have been quantified using various techniques and instruments in a number of extensive studies inside and outside cow barns as well as downwind of farms. The onsite studies calculate $CH_4$ emission rates based on ventilation rates and local $CH_4$ concentration enhancements and investigate the influence of environmental conditions on $CH_4$ emissions, such as animal activities, air temperature, and relative humidity. Ngwabie et al. (2009) and Joo et al. (2015) showed that the enhanced $CH_4$ concentrations inside a barn were mostly affected by ventilation rates, and by air temperature and relative humidity, and were negatively correlated with all the three parameters. Furthermore, the enteric $CH_4$ emissions from cows were found to increase significantly with increasing animal activities, while animal activities were observed to be negatively correlated with the indoor air temperature in the range from ~5 °C to ~20 °C (Ngwabie et al., 2011). Also, feeding has a strong positive effect on the enteric $CH_4$ emission, with peak emissions approximately 1 h after feeding in the morning and in the afternoon (Amon et al., 2001; Gao et al., 2011; Hegarty, 2013; Ngwabie et al., 2011). Feed intake and quality and manure management that may be influenced by seasonal variations also influence the $CH_4$ emissions (Zhang et al., 2005; Bernier et al., 2012; Wu et al., 2012; Moe and Tyrrell, 1979). Many studies have observed clear diurnal fluctuations in enteric $CH_4$ emissions. However, no clear seasonal variations have been measured (Amon et al., 2001; Grainger et al., 2007; Saha et al., 2014).

On the other hand, the off-site studies deploy atmospheric measurements of $CH_4$ mole fractions downwind of the farms using various sampling techniques, and then use inverse dispersion models or tracer correlations to quantify the emissions. Besides the enteric emissions from cows, manure $CH_4$ emissions can be significant and highly variable on the facility scale. Arndt et al. (2018) used three independent measurement techniques (open-path with inverse modeling, vehicle measurements with a tracer release method, aircraft measurements with the close-path method) and found that the majority of the facility-scale emissions came from the liquid manure management system. A tracer release method involves a release of known amount of tracer gas nearby the methane source. The emission rates of $CH_4$ can be determined by the ratio of the mole fraction enhancement of transected downwind $CH_4$ to that of the tracer combined with known release rate of the tracer. During the summer period these were even 3–6 times higher than emissions from the animal housing. A study on the same farms by Daube et al. (2019) confirmed that a larger fraction of the facility-site emissions comes from liquid manure storage than from the animal house using the tracer flux ratio method in a combination with airborne measurements. Furthermore, Amon et al. (2001) and Ngwabie et al. (2014) found that manure emissions represent ~20% of the total farm-scale methane emission. In the Netherlands, liquid animal manure is usually stored in cellars underneath the housing facilities, and later spread on the land regularly through the year. Given this practice, in 2019 $CH_4$ emissions from the manure management represent ~22% of the total farm emissions (Ruyssenaars et al., 2021). Therefore, the facility-scale sources, like a dairy cow farm, are challenging to quantify due to its complexity and the limitations of existing atmospheric sampling methods, and it is important to understand and take into consideration all parts of animal husbandry that potentially could contribute to the total methane emission.

Unmanned Aerial Vehicles (UAVs) are part of the scientific toolbox for some time already, mainly due to their affordable price, simple use, and wide range of applications (Nathan et al., 2015; Andersen et al., 2018; Allen et al., 2018; Shah et al., 2020). The UAV's mobility makes them capable of quantifying a wide range of point and facility-scale sources, where other measurement techniques may not be deployable. For example, Nathan et al. (2015) quantified $CH_4$ leaks from a natural gas compressor station using an open-path methane sensor on board a fixed-wing remotely controlled aircraft, and Allen et al. (2018) quantified methane fluxes from a landfill using a UAV platform with a tethered 100 m long sampling tube to a gas analyser on the ground. In this study, we aim to quantify farm-scale $CH_4$ emissions based on high-precision $CH_4$ mole fraction measurements using a recently available UAV-based active AirCore System. The UAV-based active AirCore is an innovative atmospheric sampling system that consists of a long piece of coiled tubing, a pump, and a datalogger. Air samples are pulled slowly, with very little self-mixing, into the tube by the pump during a UAV flight, and are analysed after landing. The technique can be used to make atmospheric measurements in both vertical and horizontal transects, and is suitable for near-source sampling (Andersen et al., 2018).

We have quantified $CH_4$ emissions from a dairy farm in the Netherlands using UAV-based active AirCore $CH_4$ mole fraction measurements on four individual days during the period from March 2017 to March 2019. On the last measurement day, a tracer-ratio approach was employed, with sampling and analysis performed using two mobile platforms (a van and UAV-based active AirCore). This allowed us to compare results of two different mobile sampling platforms (i.e., vehicle and UAV) and evaluate the quantification methods (mass balance and inverse Gaussian plume).

## 2. Material and methods

The $CH_4$ mole fractions were measured near a dairy cow farm, in the village of Grijpskerk, about 20 km north-west of the city of Groningen, in the northern part of the Netherland. Land use in the area is predominantly pastures and cropland, with dairy cows the dominant livestock. The farm has three main $CH_4$ sources (see Fig. 1a): a barn with dairy cows (1), a barn with other cattle (dry cows, heifers, calves) (2) and three manure cellars that are located under both barns (1 and 2). The herd on average consists of 413 cattle: 260 dairy cows (average weight ~ 650 kg), 21 dry cows, 63 heifers, and 69 calves. All animal groups are fed once per day, in the morning between 6:30 am and 8:00 am (local time). The dairy cows are fed with 24 kg of dry matter (DM) per day (45% grass silage, 40% simple concentrate, 15% corn silage), while dry cows and growing cattle (heifers, calves) with 15 kg (45% grass silage, 28% corn silage, 16% straw, 11% simple concentrate) and 7 kg (86% grass silage, 10% hay, 5% simple concentrate) of


**Fig. 1.** (a) The dairy farm and its surroundings. Barn (1) for adult lactating cows, barn (2) for young cows (Photo taken by Toine Cornelissen). (b) The flight location of the downwind flights performed on 29 March 2019. The red arrow indicates the wind direction, the red circles specify the location of two 3D sonic anemometers, and the green circle the $N_2O$ release location. The green lines indicate the projected flight tracks of the UAV, and the blue line indicates the driving path of the mobile van.

DM per day, respectively. The average milk production on the studied farm is 29.5 kg milk/cow/day.

During the period from March 2017 to March 2019, four measurement campaigns were carried out on the farm. The first three campaigns were performed using a UAV-based active AirCore system from the University of Groningen (UG). The last campaign was a joint campaign using the UG UAV-based active AirCore system and a mobile van from the Netherlands organisation for applied scientific research (TNO). In all four measurement campaigns, atmospheric mole fractions of $CH_4$, $CO_2$, CO were measured downwind of the farm, nearly perpendicular to the wind direction, while in the last campaign, atmospheric mole fractions of $N_2O$ were additionally measured by both platforms during a combined $N_2O$ tracer release. A total of 17 flights and 50 car transects were performed. Of these, 8 flights and 9 concurrent car transects were used for further analysis. Nine UAV flights were excluded from this study based on the following two reasons: (1) the plumes from the farm were not successfully captured due to an inappropriate sampling location; (2) Due to technical failures of our datalogger inside the UAV-based active AirCore box that measures crucial parameters (pressure, temperature, humidity) for the analysis of our AirCore samples. Of the car transects, only the ones coinciding with two UAV flight on 29 March 2019 were analysed. We use a combination of different approaches (discussed in Section 2.5) to quantify $CH_4$ emissions from the farm.

### 2.1. UAV–based active AirCore measurements

We have made UAV-based atmospheric mole fraction measurements using an active AirCore that is described in detail in Andersen et al. (2018). Here we only give a brief introduction to the active AirCore and show the new development on the analysis of the collected AirCore air samples.

#### 2.1.1. Active AirCore

The active AirCore used in this study is nearly identical to the one in Andersen et al. (2018), which collects around 350 mL of atmospheric air samples continuously and slowly into a ~50 m long stainless-steel coil (1/8″ outer diameter) at a flow rate of ~21 sccm. A fill gas that is spiked with CO was used to help us to identify the air samples during the analysis, i.e. its starting and ending points. After the collected air samples are analysed on a spectrometer for trace gas mole fractions, we combine the analysis results with the recorded in-flight geospatial info to retrieve mole fraction profiles along the flight track.

The collected AirCore samples were analysed using a cavity ring-down spectrometer (CRDS – $CO_2$, $CH_4$, CO, $H_2O$; Picarro Inc., CA, USA, model G2401-m) in all four measurement campaigns, and using a quantum cascade laser spectrometer (QCLS – $CH_4$, $N_2O$, $H_2O$, COS, $CO_2$, CO; Aerodyne Research Inc., MA, USA, model TILDAS-CS) in the last measurement campaign.

#### 2.1.2. Trace gas analysers

*2.1.2.1. Picarro CRDS.* Most collected air samples from the active AirCore were analysed using a CRDS analyser for mole fraction measurements of $CO_2$, $CH_4$, CO and $H_2O$, in a mobile laboratory onsite. During the first campaign, the analyser's cavity pressure was set to ~186 hPa (140 Torr), and 0.4 Hz data was collected to achieve a precision ($1\sigma$) better than 0.03 ppm for $CO_2$, 0.3 ppb for $CH_4$ and 4.3 ppb for CO, respectively. For the subsequent campaigns, we have modified the analyser's cavity pressure to ~106 hPa (80 Torr), and 0.25 Hz data acquisition. The $1\sigma$ precision was changed to 0.1 ppm for $CO_2$, 0.7 ppb for $CH_4$ and 3.6 ppb for CO, respectively. A single calibration gas was used to correct the possibly small drift of the CRDS measurements (Andersen et al., 2018).

*2.1.2.2. Lab-based QCLS.* During the last campaign on 29 March 2019, air samples collected during 3 out of 6 AirCore flights were analysed on a dual-laser QCLS for mole fraction measurements of $CH_4$, $N_2O$, CO, $CO_2$, COS and $H_2O$. The first laser of the QCLS ($CH_4$, $N_2O$, $H_2O$) scans between wavenumbers 1275.30 and 1275.75 and the second laser (COS, $CO_2$, CO) scans between 2050.30 and 2050.95. The cavity of the analyser is maintained at a pressure ~ 66 hPa (50 Torr) and a temperature 25 °C. The spectrometer attains a precision ($1\sigma$, individual samples at 1 Hz) better than 0.45 ppb for $CH_4$, and 0.1 ppb for $N_2O$. Drift is in the order of 1 ppb per hour for both species. The analysis of a single AirCore takes approximately 15 min. The calibration of measured profile data was performed against four standards that are traceable to the WMO 2007, 2004A, 2004A and 2006A scales for CO2, CH4, CO, $N_2O$, respectively, and each was measured repeatedly before and after the sample analysis. Linear QCLS response functions were obtained by fitting measurements of the standards to assigned values after linearly interpolating these measurements in time. The obtained time-varying response functions were applied to analysed samples.

#### 2.1.3. Spatial resolutions of AirCore measurements

As discussed in Andersen et al. (2018), the spatial resolution of the UAV-based active AirCore is determined by three factors; analyser smearing effect, GPS uncertainties, molecular diffusion and Taylor dispersion. The spatial resolution is mostly dominated by the air mixing inside the analyser cavity, causing smoothening of the actual signal. When the air samples were not immediately analysed after the flight, the molecular diffusion became also an important factor.

The Picarro CRDS cavity volume is 35 mL. It was maintained at 140 Torr (186 hPa) and 80 Torr (106 hPa), making the effective cavity volume roughly 5.5 mL and 3.2 mL, respectively. The volume of the lab-based QCLS cavity is 150 mL, with the effective cavity volume around 10 mL when the cavity pressure is maintained at 50 Torr (66 hPa). For the UAV speed between 2.2 and 2.7 $ms^{-1}$, the spatial resolution of AirCore measurements with Picarro ranges from 25 to 52 m for $CH_4$. The spatial resolution

of AirCore measurements with the lab-based QCLS is ~57 m for $CH_4$, for the average UAV speed of 2.6 $ms^{-1}$.

#### 2.1.4. UAV flights

The UAV flights were performed either upwind or downwind of the farm, with approximately constant speed along a flying track perpendicular to the wind direction (Fig. 1b). Furthermore, several altitudes were sampled during each flight and the tracks were extended to cover the entire $CH_4$ plume from the farm, although a full capture of the plume may not be achieved when large deviations from the mean wind occur. A summary of the flight info of five downwind flights is shown in Table 1. The flights took between 7 and 13 min, the mean UAV speeds ranged between 2.2 and 2.7 m/s, and the distances of the flight tracks to the center of barn (1) are between 108 m and 291 m. Most flights were performed around noon except one morning flight on 29 March 2019.

### 2.2. Mobile van measurements

A van was used as a second mobile platform to measure the $CH_4$ mole fractions downwind of the source. Ambient air was sampled through a stainless-steel central inlet tube with a diameter of 60 mm at the front of the trailer at 3 m height, from which a 1/4″ PE tube goes to the instrument. $CH_4$ and $N_2O$ were measured continuously with a flow rate of 6 L/min and a precision of 1 and 0.1 ppb, respectively. Precision was reported as three times the standard deviation of six minutes' averages of reference gas measurements. In the car GPS, gas concentrations from various analysers and data from both on-board (Vaisala RX500) and remotely located meteo set (Gill 3D Windsonic) are also collected simultaneously at 2 Hz. Both $CO_2$ and CO data clearly show when the car catches its own exhaust plume, for example when standing still with the wind from behind the car – these data are not used.

#### 2.2.1. Mobile QCLS $CH_4$ and $N_2O$ analyser

The analyser in the van is a Tunable Infrared Laser Direct Absorption Spectroscope (TILDAS) using a combined quantum cascade laser (QCL) and interband cascade laser (ICL) (Aerodyne Research Inc., Billerica, US), referred to as mobile QCLS. The unit is similar to the one used at the UG. It measures $CH_4$, $C_2H_6$, $N_2O$, $H_2O$, $CO_2$, CO, methanol and formaldehyde. The system has a 72 m multipass cell with a volume of 500 mL that is operated at a pressure of ~53 hPa (~40 Torr) and a temperature of ~303 K. The delay time of the system and the inlet line is ~2 s and the 90% rise time to a step in the concentration is ~0.5 s. Two-point calibrations were done 3 or 4 times during the measurement day using 1900 and 5000 ppb $CH_4$ and 300 and 500 ppb $N_2O$ in air mixtures that were calibrated against ICOS calibration standards. In these calibrations, $CH_4$ had a precision ($1\sigma$, 2 Hz) of ~2 ppb, and $N_2O$ ~ 0.5 ppb. With $CH_4$ and $N_2O$ peak concentrations of about 200–400 ppb above the background this implies a signal to noise ratio of 1/100. Instrument-related uncertainty is thus much smaller than the plume-to-plume and turbulence-induced variabilities that are in general in the order of 20–40% depending on meteorological conditions.

#### 2.2.2. Driving paths

Driving along the provincial road (Fig. 1b) the car passed through the methane plume from the farm 50 times. On the busy road, driving speed cannot be much lower than 60 km/h and single plume crossings therefore are obtained in 10–15 s. The $CH_4$ mole fractions measured by the mobile QCLS are later compared with a series of simulations of the Gaussian plume model.

### 2.3. Meteorological measurements

The wind measurements for the first three campaigns were taken from the 3 nearest meteorological stations of the Royal Netherlands Meteorological Institute (KNMI), other than that, two other instruments were used to measure the wind; a radiosonde (3 May 2018) and two 3D sonic anemometers were used onsite during the last campaign (29 March 2019). The nearest KNMI stations are located in Eelde, Leeuwarden and Lauwersoog, and are located ~30 km, ~ 39 km, and ~25 km away from the farm, respectively.

#### 2.3.1. 3D sonic anemometer

During the joint campaign (29 March 2019) with TNO, two 3D sonic anemometers were used to measure the wind at the farm itself (Fig. 1b). The data was obtained with WindMaster Pro (Gill Instruments) ultrasonic anemometers at heights of ~2 m (UG) and ~1.8 m (TNO), with a sampling frequency of 10 Hz (UG) and 20 Hz (TNO).

#### 2.3.2. Radiosonde

During the second campaign (3 May 2018), a lightweight radiosonde (Sparv Embedded AB, Sweden, model S1H2-R) was used to measure the vertical profiles of ambient temperature, relative humidity, pressure, wind speed and wind direction and GPS data. We launched the radiosonde using a tethered weather balloon that was secured to a fishing rod, flying up to ~50 m. The radiosonde was reused and 2 radiosonde profiles were made close to the time of the downwind flight (~20 min after the flight). The in-situ radiosonde measurements were sent to a receiver connected to a laptop on the ground.

### 2.4. $N_2O$ tracer release

A tracer release experiment was performed during the flights on 29 March 2019. The experiment lasted ~5 h, from 10:48:00 (UTC) to 15:28:30 (UTC), during which one UAV flight was made coinciding with four driving paths. The released tracer was $N_2O$, using a pure $N_2O$ cylinder equipped with a pressure reducer and critical orifice. The release rate was 0.8 ± 0.04 g/s, which was released close to the farm indicated in Fig. 1. b. Note that there may be $N_2O$ emissions from the farm itself; however, they were small when compared with the signal from the $N_2O$ tracer release. Before the start of the $N_2O$ release experiment, the TNO van measured $N_2O$ background of 332.1 ± 0.4 ppb. The size of our observed signal is significantly larger than the variation of the background of 0.4 ppb (see Fig. S8). Therefore, the impact of the possible $N_2O$ emissions from the farm on the tracer release method was neglected. With this, we also assumed that the possible $N_2O$ emissions from the farm did not vary significantly during the tracer release experiment. In the end, to quantify $CH_4$ (or $N_2O$) emission rates we need a dispersion model, which is discussed in Section 2.5.

**Table 1**
Summary of the flight info of 5 downwind flights between March 2017 and March 2019 (3 upwind flights are excluded from this table).

| | 27 March 2017 | 3 May 2018 | 19 October 2018 | 29 March 2019 | |
|---|---|---|---|---|---|
| Flight time [min] | 7 | 12 | 11 | 10 | 11 |
| Take off [hh:mm:ss] [UTC] | 13:32:27 | 11:43:50 | 12:23:30 | 09:57:03 | 12:50:27 |
| Landing [hh:mm:ss] [UTC] | 13:39:48 | 11:56:05 | 12:34:51 | 10:07:10 | 13:01:56 |
| Mean UAV speed [m/s] | 2.7 | 2.4 | 2.2 | 2.2 | 2.6 |
| Distance [m] | 108 | 117 | 126 | 291 | 221 |

### 2.5. Quantification of $CH_4$ fluxes

#### 2.5.1. Mass balance approach

The $CH_4$ mole fraction measurements from the UAV-based active AirCore were used to calculate the $CH_4$ mole fraction enhancement over the background downwind of the farm. The $CH_4$ emission rates from the farm are determined using a mass balance approach (MBA) that is similar to the ones used in Nathan et al., 2015 and Allen et al., 2018, which is given by the following equation:

$$Q_{CH_4} = \overline{v}\, cos\, \overline{\theta} M_{CH_4} \overline{n}_{dryair} \sum\sum \Delta c \Delta x \Delta z, \quad (1)$$

$$\overline{n}_{dryair} = \frac{P\,(1-H_2O)}{R\,T} \quad (2)$$

where $\overline{v}$ is the mean horizontal wind speed in meter, the angle $\overline{\theta}$ is the angle between the mean wind direction and the direction normal to the downwind flight track, $M_{CH4}$ is the molecular mass of methane, $\Delta c$ is the $CH_4$ mole fraction enhancement over background, while $\Delta x$ and $\Delta z$ are the horizontal and the vertical increments of the integration plane, respectively. The term $\overline{n}_{dryair}$ is the molar density of dry air, which is calculated based on the onboard measurements of ambient pressure (P), temperature (T) and relative humidity (RH). The mole fraction of water vapor ($H_2O$, in percent) is calculated using ambient T and RH, and R is the universal gas constant.

*2.5.1.1. $CH_4$ background.* Significant variations have been observed in the $CH_4$ background between the flights on a single day. To understand those variations, measured concentrations during flights upwind and downwind of the farm were compared with continuous measurements from the nearby atmospheric station Lutjewad. The station is located ~15 km north of the farm, on the northern coast of the Netherlands, next to the Wadden sea dike, where $CO_2$ and $CH_4$ are continuously monitored at a 60 m tower. We have assessed the background $CH_4$ values derived as the mean and the 10th percentile of the upwind flight and the Lutjewad measurements, and the 10th percentile of the downwind flight. A temporal change of similar magnitude in the derived background at both locations was observed (Fig. S2), indicating that the temporal change of the background is dominated by processes at a scale of tens of kilometers or more, e.g., due to a change of boundary layer height. Therefore, we use the background value derived from the 10th percentile of the downwind flight $CH_4$ measurements, instead of those derived from the upwind flight data on the same day, to avoid introducing a bias to the background due to temporal change.

*2.5.1.2. Kriging interpolation.* To integrate the $CH_4$ mole fraction enhancements, we first spatially interpolate the data onto a two-dimensional plane to obtain estimated $CH_4$ mole fraction enhancements at locations where observations were not made, by using the Kriging geospatial interpolation method (Myers, 1991) (Fig. 2b). The Kriging method considers experimental variograms, covariograms, and correlograms, which are the basis to determine the correlation length. The experimental variogram represents the spatial distribution of the data, using a measure of variability between pairs of points at various distances, while the correlogram estimates the correlation between pairs of points. An experimental variogram of sampled $CH_4$ mole fractions enhancements is determined for each flight. In this study, the experimental variogram is based on variograms in both horizontal and vertical directions, so-called composite variogram. Based on the experimental variogram and correlogram, the best model fit is determined together with a correlation length that is afterward used for Kriging prediction. Therefore, to minimize uncertainty these parameters need to be defined in a way that suit our sampling technique the best.

*2.5.1.3. Uncertainties.* Based upon the variability and uncertainty in each variable of the mass balance equation (Eq. (1)), we derive the total uncertainty (Eq. (3)) by error propagation. Furthermore, the wind speed ($\delta\overline{v}$) and wind direction ($\delta\overline{\theta}$) uncertainties consist of measurement uncertainty and temporal variation that are summed up in quadrature. Temporal variability is estimated as the standard deviation (1σ) of a variable (mean wind speed, mean wind direction or mean molar density of dry air) over the time. The uncertainty of enhanced $CH_4$ mole fraction ($\delta\Delta c$) is determined as a sum of measurement uncertainty and standard deviation (1σ) of kriging prediction, while the uncertainty of the molar density of dry air ($\delta\overline{n}_{dryair}$) includes only the temporal variability (1σ).

$$\delta Q_{CH_4} = \sqrt{\left(\frac{\partial Q_{CH_4}}{\partial \overline{v}}\delta\overline{v}\right)^2 + \left(\frac{\partial Q_{CH_4}}{\partial \overline{\theta}}\delta\overline{\theta}\right)^2 + \left(\frac{\partial Q_{CH_4}}{\partial \Delta c}\delta\Delta c\right)^2 + \left(\frac{\partial Q_{CH_4}}{\partial \overline{n}_{dryair}}\delta\overline{n}_{dryair}\right)^2} \quad (3)$$

$$\begin{aligned} \delta\overline{v}, \delta\overline{\theta} &= \sqrt{measurement\ uncertanity_{v,\theta}{}^2 + temporal\ variation_{v,\theta}{}^2} \\ \delta\overline{\Delta c} &= measurement\ uncertanity_{\Delta c} + st.dev\left(kriging\ prediction_{\Delta c}\right) \\ \delta\overline{n}_{dryair} &= st.dev\left(\overline{n}_{dryair}\right) \end{aligned} \quad (4)$$

The interpolated downwind $CH_4$ concentration includes the two main contributors of Kriging uncertainty - Kriging prediction, and the grid resolution.

Prior to Kriging interpolation, an experimental variogram of sampled $CH_4$ mole fractions was determined for each flight. Once the experimental variogram is calculated, the remaining task is to find parameter values (range, sill, nugget), for the model that yields the best fit to experimental variogram. The spherical fit was used as a standard fit to our experimental

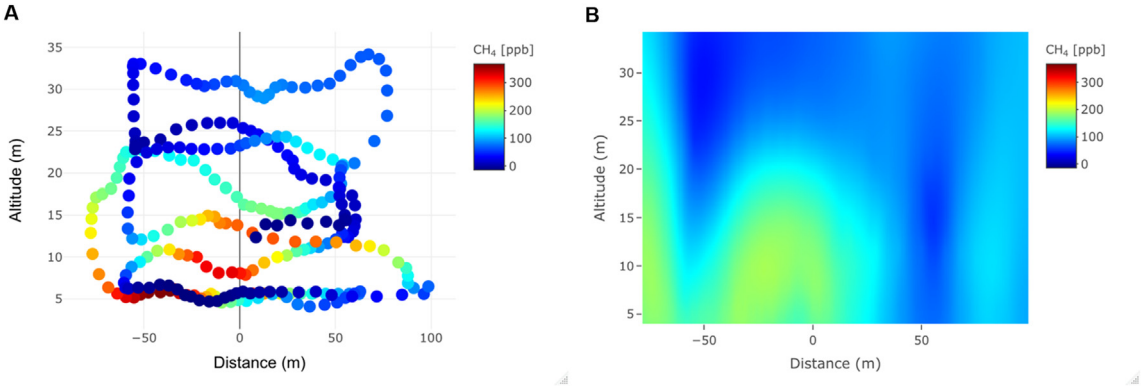


**Fig. 2.** The measured and Kriged $CH_4$ enhancements over background for the flight on 29 March 2019. (a) 2D plot of $CH_4$ enhancements distributed in space. (b) Kriged $CH_4$ enhancements.

variograms. The composite's correlation length is dominated by the horizontal variogram due to a poor spatial resolution of the vertical variogram. The Kriging interpolation was performed using the R package 'gstat' for Spatial and Spatio-Temporal Geostatistical Modeling, Prediction, and Simulation (version 2.0-7). The high horizontal correlation length is partly due to the spatial resolution of AirCore $CH_4$ mole fraction measurements. Furthermore, the grid size is another source of uncertainty when it comes to the flux plane for the Kriging interpolation. The grid resolution 180 × 180 was used as a standard grid resolution for all flights, where the typical size of our flux plane was ~180–270 m horizontal by ~30–100 m vertical. Furthermore, emission rates were estimated for two flights on 29 March 2019 for three different grid resolutions, 20 × 20, 60 × 60, 180 × 180, to assess the flux sensitivity to the grid resolution.

#### 2.5.2. Manure emissions

The dairy farm produces mostly slurry manure, with a small amount of solid manure (~200 tons). Slurry manure is collected in three cellars underneath barns (1) and (2), of which two separate cellars are located under barn (1) and one underneath barn (2). Solid manure is stored outside, on the southwestern side of barn (2). Usually, the cellars are emptied three times per year (March, May/June, August) during the growing season, to be spread into the fields. From August to February manure is collected and stored in the cellar before it is used in the field. The total capacity of the three cellars is around 7000 tons.

Knowing the approximate amounts of slurry manure that were taken out of the cellars in March, May and August (information provided by the farmer) from March 2017 to March 2019, we estimated the amount of slurry manure that was present in the cellars on the individual campaign days to be in a range from 3000 to 4600 tons. The slurry manure production was assumed to be constant, in a range from 630 to 850 tons per month, or equivalent to 7560 to 10,200 tons per year. The manure production range was determined based on the manure production rates from the Dutch National Inventory report for different cattle age (Coenen et al., 2014), and the estimated production rate provided by the farmer (see the details in Appendix Table S2).

In this study, an equivalent of 305 dairy cows (average weight ~650 kg) or an equivalent of 397 AU (500 kg live mass per AU) was used in the conversion from source strength (g $CH_4$/s) to emission rate per cow per day (kg $CH_4$/cow/d) for both enteric fermentation and manure onsite. According to the Dutch National Inventory Report, 2021 (Ruyssenaars et al., 2021) dry cows emit ~57% of the amount of $CH_4$ compared to mature dairy cows, while growing cattle about ~25%. We have used the emission ratios to convert 21 dry cows and 132 growing cattle to an equivalent of 12 and 33 mature dairy cows, respectively. Given the estimated total amount of slurry manure onsite and the $CH_4$ emission factor (39 kg $CH_4$/cow/year) for manure management in the Netherlands (Ruyssenaars et al., 2021), we estimated the $CH_4$ emission rates per cow from manure onsite for each individual campaign from March 2017 to March 2019 using Eq. (5). The $CH_4$ emission factor for manure management in the Netherlands has an uncertainty of ±38% (Ruyssenaars et al., 2021) that has been taken into the account to the total uncertainty of the manure $CH_4$ emission rate. With this approach, we have assumed that the emission rate from manure is proportional to the amount of manure, and is constant throughout the year despite the status of the manure. The emission from solid manure onsite is ignored due to the fact that the emission rate of solid manure is much lower compared to that of slurry manure (Saunois et al., 2016; Coenen et al., 2014), and the amount of solid manure onsite is much less than the estimated amount of slurry manure onsite.

$$\textit{Manure onsite emissions}_{CH_4} = 39\ kg\ CH_4/cow/year \cdot \frac{manure\ onsite}{total\ manure\ in\ one\ year} \quad (5)$$

#### 2.5.3. The inverse Gaussian plume approach (IGA)

For the mobile van measurements, a Gaussian plume model was used to simulate the concentration levels at the transect. It estimates the concentration of the plume that is transported downwind of the source (Hensen, 2011).

$$C(x,y,z) = \frac{Q}{2\pi \bullet u \bullet \sigma_y \bullet \sigma_z} \bullet e^{\frac{-y^2}{(2\bullet\sigma_y)^2}} \bullet \left( e^{\frac{-(z-h_s)^2}{(2\bullet\sigma_z)^2}} + e^{\frac{-(z+h_s)^2}{(2\bullet\sigma_z)^2}} \right) \quad (6)$$

The concentration $C$, of a pollutant at $(x,y,z)$ from a point source with the height of the emission, $h_s$, is given by Eq. (6).

In Eq. (6), $x$ is the distance parallel to the wind direction ($m$), $y$ the distance perpendicular to $x$ ($m$) and $z$ the height above the ground ($m$), $Q$ the source strength ($g/s$), and $u$ the mean wind speed that affects the plume ($m/s$). The dispersion parameters in the crosswind and the vertical directions, $\sigma_y(m)$ and $\sigma_z(m)$ respectively, depend on the distance to the source, on the degree of turbulence of the atmosphere, the roughness length of the surface $z_0$, and on the time-scale $T(h)$ that is used for averaging. For $\sigma_y$ and $\sigma_z$, the following functions (Hensen, 2011) apply:

$$\begin{aligned} \sigma_y &= a \bullet x^b \bullet z_0^{0.2} \bullet T^{0.35}, \\ \sigma_z &= c \bullet x^d \bullet (10 \bullet z_0)^e \bullet T^{0.35}, \\ e &= x^{-0.22}. \end{aligned} \quad (7)$$

Turbulence in the atmosphere mixes clean air with polluted air, which results in a lower measured concentration of a pollutant in the plume. Parameters A, B, C, and D, presented in Table S1, depend on the stability class (Hanna, 1981). Class A corresponds to a "very unstable" atmosphere, while class F corresponds to a "stable" atmosphere.

In the model, multiple sources are placed at different locations over the source area that is being observed. In the end, the total concentration $C$ at location $(x,y,z)$ is a sum of the contributions of all individual sources. Therefore, the emission rate is derived from the ratio (Eq. (8)) of the integrated concentration of the measured and modelled concentration plumes multiplied with the source strength of 1 $gs^{-1}$ ($Q_{model}$).

$$Q_{CH_4} = Q_{model} \bullet \frac{\int observed\ plume}{\int modeled\ plume} \quad (8)$$

#### 2.5.4. Single or multiple sources

The model was run with different initial parameters, in this particular case, the number of sources per barn was varied. The first run consisted of one source, positioned in the center of the barn (1) (Fig. 3a). Then the second run included nine individual sources spread over the barns (1) and (2) in a grid (Fig. 3b), therefore, the idea is to improve plume simulations by setting multiple sources in the model.

## 3. Results and discussion

### 3.1. Meteorological data

This section presents the meteorological data that were obtained from different instruments onsite and at nearby KNMI stations (mean values of three KNMI stations for each campaign) (Fig. 3). As expected, variability in both horizontal wind speed (33–63%) and wind direction (25–46%) from KNMI stations are significantly higher compared to that of onsite measurements of horizontal wind speed (21–37%) and wind direction (5–12%). Knowing that accurate wind measurements and its variability are important for the estimation of fluxes (Allen et al., 2018), radiosondes and 3D sonic anemometers were used in May 2018 and March 2019, respectively.

A total of 4 radiosonde launches were performed, out of which only 2 were launched within ~20 min from the downwind flight period in May 2018. Their vertical profiles of both wind speed and wind direction can be found in Fig. S3). The wind speeds calculated from three KNMI stations and from the radiosonde measurements agree within their uncertainties; however, the wind directions differ significantly, which is likely due to spatial variability that affects the wind directions more than the wind speed. For the flight in May 2018, we have used the wind speed and wind direction


**Fig. 3.** Distribution of sources across barns (1) and (2), the red circle indicates the location of each individual source. (a) Single source. (b) Grid made of multiple sources, in this case, nine individual sources per each barn.

measurements from the radiosonde because we wanted to have an accurate onsite wind measurement. Regarding the wind measurements from the two 3D sonics in March 2019, for the entire 6 h measurement period, we found a mean difference of 0.7 ± 0.6 $ms^{-1}$ and 5 ± 35 deg for horizontal wind speed and wind direction, respectively (Fig. S4). The difference is likely due to the spatial variability of the wind field since the two 3D sonic anemometers were placed on the opposite sides of the farm (see Fig. 1a) with a distance of ~270 m between them. To account for the variability, we have used the mean wind speed and wind direction of the two 3D sonics. For the two flights in March 2017 and October 2018, the wind direction and the wind speed were calculated as a mean value from the three nearby KNMI stations. The differences in wind speed and direction are accounted for in the overall error estimate we present in Section 3.2.1 below.

### 3.2. Farm-scale emission rates

The total $CH_4$ emission rates from the farm determined using the mass balance approach (Eq. (1)) are shown in Fig. 5. The estimated emission rates vary by a factor of ~2.5 over the campaigns, in the range of 1.1–2.4 g/s and the average emission rate over all quantifications is 1.7 ± 0.6 g/s. Furthermore, in March 2019, compared the emission rates calculated based on the KNMI data versus the onsite wind measurements the difference in the emission rates was for the first flight ~23% lower with the KNMI data, while ~10% higher for the second flight. The sources of $CH_4$ include both the cows and the manure in storage on the farm. Since the manure is stored under the barns, the emissions from the manure and from the cows are basically co-located and cannot be distinguished from downwind $CH_4$ measurements. The variations of the emission rates over time may be due to three factors: (1) uncertainties of the estimates, (2) changing amount of manure on the farm; (3) changing emission rates of cows. These are further discussed in the following sub-sections.

#### 3.2.1. Uncertainties of the estimates

We first show the uncertainties of the estimates based on the propagation of the mass balance equation (Eq. (3)). Following this, we present the uncertainties associated with the grid resolutions and the Kriging parameters through a series of sensitivity studies.

The total uncertainties of the estimated emission rates determined based on Eq. (3) and the uncertainties contributed by individual components are shown in Table 1. For all flights, the two components of the horizontal wind speed uncertainty and the uncertainty of the angle $\bar{\theta}$ are dominating factors, which have been significantly improved in more recent flights with onsite continuous wind measurements from anemometers that are practical to implement. The earlier two flights in March 2017 and October 2018 have much larger uncertainties compared to those in May 2018 or March 2019, which could be explained by larger wind uncertainties due to the wind variability between the KNMI stations (presented in Section 3.1). The uncertainties associated with the estimate for the flight in May 2018 are also relatively large compared to those in March 2019. This is because the radiosonde used in May 2018 provides only a vertical profile that represents both temporal and vertical variabilities, while the 3D sonics used in March 2019 provide continuous measurements near the surface and the vertical variability is not considered. From this aspect, the uncertainties associated with the estimates for the flights in March 2019 may be underestimated. The two components associated with the uncertainties of $\bar{n}_{dryair}$ and $\Delta c$ are 2–5 orders of magnitude smaller compared to those associated with the wind speed and the angle $\bar{\theta}$, are negligible (see Table 2).

To assess the uncertainty associated with the Kriging grid resolution, we decreased the grid resolution (180 × 180) for all five downwind flights by a factor 3, which results in an increase of 2–3% in the quantified emission rate, while by a factor 9 in a 5–14% increase. Nathan et al., (2015) assessed the uncertainty associated with the Kriging grid resolution in a similar study and found a within 4% increase or decrease with a change of the grid resolution by a factor 2. The increase of our sensitivity results is slightly smaller than in Nathan et al. (2015) with the variation by a factor 3 of the grid resolution. Note that our grid resolution of 180 × 180 corresponds to a spatial resolution of 1–1.5 m in the horizontal direction and 0.2–0.6 m in the vertical direction, which is already quite high, and is significantly higher than the spatial resolution of 11.6–24.4 m in the horizontal direction and 1.2–7.2 m in the vertical direction used in Nathan et al., 2015. Indeed, when our grid resolution was further increased, we found insignificant change in the estimated emissions. Because the observed AirCore $CH_4$ measurements are smoothed mainly due to the measurement cell smearing effect during sample analysis, our experimental correlation length may not represent the true correlation length of the $CH_4$ plume. In fact, the spatial resolution of our AirCore measurements is estimated to be ~25–57 m, which is comparable to the estimated correlation length of ~11–28 m. To find the true correlation length of the $CH_4$ plume, AirCore observations are deconvolved (Andersen et al., 2021) by accounting for the smearing of the signal in the CRDS measurement cell. Furthermore, the goal of the deconvolution is to recreate the original signal as it existed before the AirCore samples were analysed. The results show that the flux estimate for the first flight on 29 March 2019 has increased ~15%. The increase is due to both the background difference (52%) and the correlation length difference (48%). Furthermore, for the UAV approach, the nonsimultaneous sampling in the vertical direction of the plume is one of the main limiting factors to achieving accurate estimate of the $CH_4$ emissions from the farm. To this end, the use of multiple UAVs would improve the spatial coverage of the measurements. If multiple UAVs are positioned in a way that they are able to sample the plume at different altitudes simultaneously, the uncertainty of the emission estimate will be significantly reduced.

**Table 2**
An overview of the estimated $CH_4$ fluxes and their total uncertainties and the uncertainties due to individual components (all units are in g/s) based on the propagation of the mass balance equation for the five downwind flights from March 2017 to March 2019.

| | March 2017 | May 2018 | October 2018 | March 2019 (#1) | March 2019 (#2) |
|---|---|---|---|---|---|
| Total flux | 2.1 | 1.7 | 2.4 | 1.3 | 1.1 |
| Total uncertainty | 1.9 | 0.8 | 1.5 | 0.4 | 0.4 |
| $\bar{v}$ uncertainty | 1.3 | 0.6 | 1.1 | 0.4 | 0.3 |
| $cos\,\bar{\theta}$ uncertainty | 1.4 | 0.5 | 1.0 | 0.1 | 0.2 |
| $\bar{n}_{dryair}$ uncertainty | $1.3{\cdot}10^{-2}$ | $3.4{\cdot}10^{-3}$ | $2.7{\cdot}10^{-3}$ | $3.6{\cdot}10^{-5}$ | $3.4{\cdot}10^{-5}$ |
| $\Delta c$ uncertainty | $7.7{\cdot}10^{-5}$ | $5.9{\cdot}10^{-5}$ | $5.2{\cdot}10^{-5}$ | $1.5{\cdot}10^{-3}$ | $1.9{\cdot}10^{-3}$ |

*3.2.2. Emission factors of enteric $CH_4$*

Based on the determined farm-scale emission rates (Fig. 4) and the animal unit on the farm, the emission factors of enteric $CH_4$ emissions of dairy cows were derived. The farm-scale emissions include two major components, enteric and manure $CH_4$ emissions. Since the amount of slurry manure in the cellars under the barns on the individual campaign days does not vary significantly between the different campaigns (Fig. 6a), we assume that manure $CH_4$ emissions do not vary significantly between our campaigns based on our observations, and have subtracted the estimated emission factors of manure onsite from the total quantified farm emissions to derive the emission factors of enteric $CH_4$ emissions (Fig. 6b).

The $CH_4$ emission factors from enteric fermentation range from 0.20 to 0.51 kg $CH_4$/AU/d. The emission factors in 2017 and 2018 are higher compared to those in 2019, which may not be significant when considering the relatively large uncertainties in 2017 and 2018. Since the total animal unit on the farm did not change during the study period and the estimated manure emission factors onsite vary in a small range, the variation in the emission factors mainly reflects the difference in the determined emission rates from the farm. The $CH_4$ emission factors obtained in this study are within the range of the previously reported values (Table 3): 0.20–0.25 kg$CH_4$/AU/d (Jungbluth et al., 2001), 0.17–0.36 kg$CH_4$/AU/d (Ngwabie et al., 2011), 0.26–0.35 kg$CH_4$/AU/d (VanderZaag et al., 2014), 0.34–0.46 kg$CH_4$/AU/d (Arndt et al., 2018). The mean $CH_4$ enteric emission factor found in this study is 162 ± 61 kg $CH_4$/cow/yr (124 ± 47 kg $CH_4$/AU/yr), which provides an independent verification of the estimated value of 117 kg$CH_4$/cow/year from enteric fermentation for Western Europe (IPCC, 2006), and the estimated value of 136 kg $CH_4$/cow/yr in the Netherlands in 2019 (Ruyssenaars et al., 2021). Furthermore, we found that the reported enteric emission factor for West Europe is comparable to that for North Europe, and is lower than that for North America (see Fig. 7). Note that the enteric emission factors used in this comparison are all based on atmospheric measurements, and large variations exist among different studies.

Our estimated emission factors are based on short-period measurements on four individual days. Previous studies based on continuous monitoring have reported a spike in $CH_4$ emissions after feeding. Since our observations were made in local time between 11:00 and 15:00, which were a few hours after the morning feeding, our estimates are likely not affected by the relatively large variations due to feeding. However, all our measurements were done only during daytime, and nighttime emissions from cows may be lower due to the reduced nocturnal activity of the cattle (Jungbluth et al., 2001; Amon et al., 2001; Gao et al., 2011), in this aspect, our results may overestimate.

The estimated methane emission factors of manure onsite range from 13 to 20 kg$CH_4$/cow/yr, which were derived by scaling the emission factor of 39 kg $CH_4$/cow/yr (Ruyssenaars et al., 2021) with the fraction of manure onsite; however, IPCC (2006) suggests an emission factor of 23 kg $CH_4$/cow/yr for Western Europe (average annual temperature ~ 11 °C). The main cause of the discrepancy comes from the different approaches that are used to determine the $CH_4$ emission factors from manure management, i.e., IPCC uses the Tier1 approach that incorporates the manure practices and the average annual temperature in a large region, while the Dutch national inventory (Ruyssenaars et al., 2021) applies the country-specific emission factor that focuses on the Netherlands' manure management system conditions (storage temperature and period) and manure characteristics (volatile solids excretion and maximum $CH_4$ producing potential). We acknowledge that it is a major assumption that manure emissions are proportional to the amount of manure onsite, even though the status of the manure and the manure emission rate may vary through the year. As the manure was stored directly under the cow barns and the cows were inside the barns during all measurement days, our measurements were not able to separate enteric fermentation from manure emissions. Further studies are encouraged to independently determine the emission rates of enteric and manure emissions from cow farms.

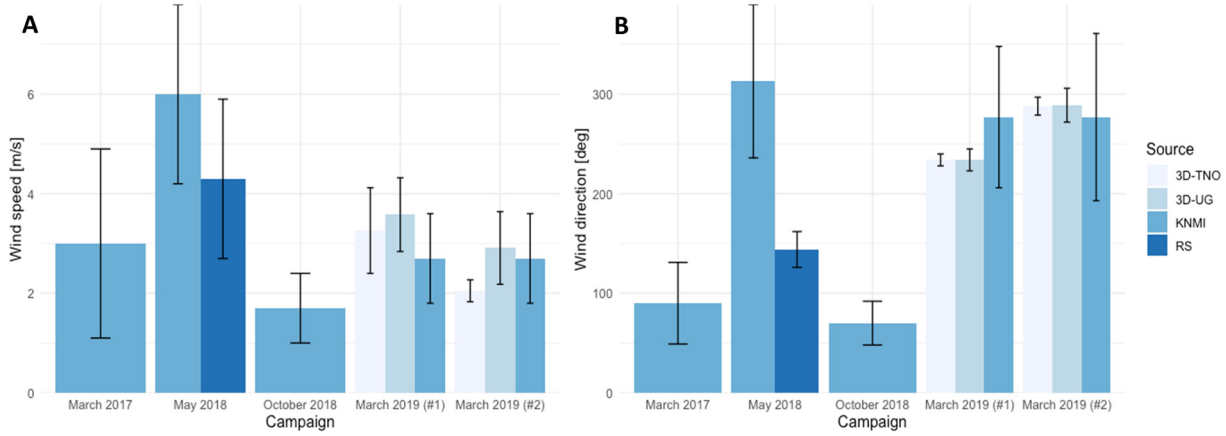


**Fig. 4.** An overview of horizontal wind speed (m/s) and wind direction (deg) during 5 downwind flights, March 2017–March 2019, obtained from KNMI stations (KNMI), radiosonde launches (RS) and 3D sonic anemometers (3D-UG, 3D-TNO).

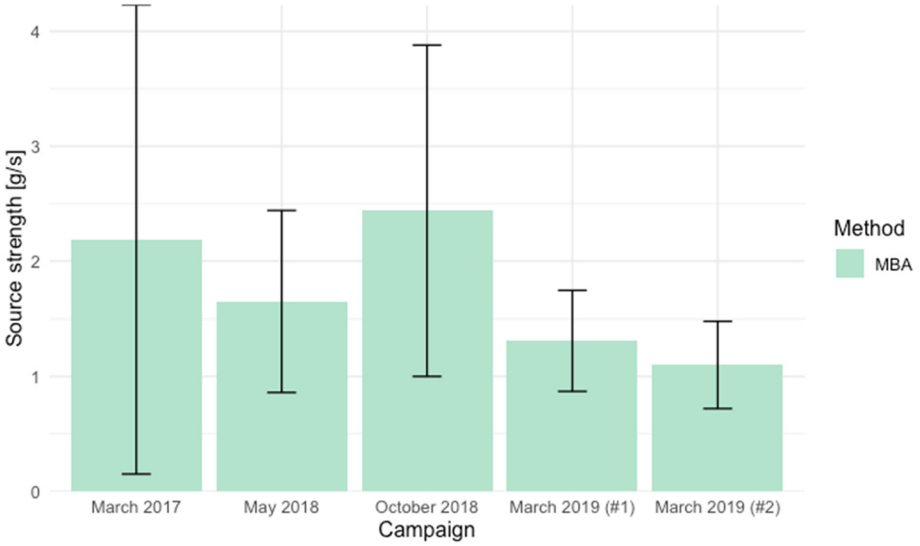


**Fig. 5.** Estimated source strength from the Grijpskerk farm for five individual campaign flights from March 2017 to March 2019, using a mass balance approach (MBA). The error bars represent the uncertainty range of estimated source strength.

### 3.3. $CH_4$ estimates using the inverse Gaussian approach

In total, around 50 $CH_4$ plumes were scanned by the van; however, in this evaluation, we focus on the analyses of the $CH_4$ plumes that were measured simultaneously with the drone sampling. Five plumes were measured with the van during the first flight, and four plumes during the second flight (Fig. S6).

Observed measurements were compared with a series of Gaussian plume model simulations to determine the $CH_4$ emission rate from the dairy cow farm. For the model we used the mean wind speed and wind direction data form the two 3D sonics, and the geospatial info from a GPS receiver in the car. The plume was simulated using one point source placed in the center of the barn (1) at a height of 5 m above the ground. On 29 March 2019, we had a sunny day with 2/8 cloud coverage and a windspeed of 2–4 m/s. For the model, a Pasquill stability class D (neutral) was used. A parameter that is not well known is the initial dispersion after exiting the cow barn, and sensitivity runs were done with initial vertical plume dispersion applying a $\sigma_z$ offset (0 m, 5 m, 10 m). When the width of the modelled plume is in agreement with that of the measured $CH_4$ plume, the model is suited for the integration of both measured and modelled plumes (Eq. (8)). In our case, when the vertical dispersion $\sigma_z$ offset was equal to 0 m, the modelled plumes best matched with the observed plume. Therefore, our estimates before correction for the first and second transects are 2.2 ± 0.2 $gs^{-1}$, and 1.0 ± 0.3 $gs^{-1}$. As an alternative to the single source plume simulation, 18 individual sources were placed across the barns (1) and (2) in the second model run. The emission estimate for the first and the second transects increase between 1 and 2%, while their uncertainties decreased by 4–10%. Given the good agreement in the estimated emissions between the two simulation approaches, a single source is used to calculate the emission rates of all transects.

The average emission rate of the first set of mobile van transects agrees within 51% with the first UAV-based active AirCore flight, while the estimate of the second set of transects agrees within 17% for the second flight. Average to poor agreement between the two sets of mobile van transects and the two UAV flights may be caused by the short UAV sampling time (~10 min) and the limited number of transects (first set: 5 transects; second set: 4 transects) by the van to constrain atmospheric variability (Caulton et al., 2018). Possible causes of the discrepancy between the UAV-based active AirCore and mobile van measurements are described more thoroughly in the following section.

### 3.4. Tracer release experiment

When compared to the known release rate of 0.8 $gN_2O/s$, the estimated emission rates agree within 22% for the mass balance approach (MBA) with one UAV flight, and within 4% for the Gaussian plume model (IGA) with

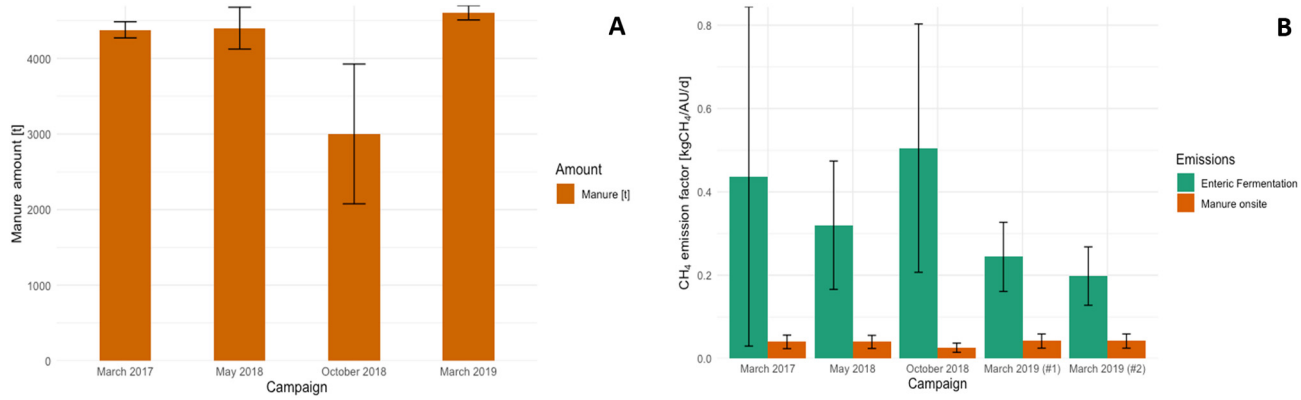


**Fig. 6.** Split of the $CH_4$ emission factors in enteric and manure emissions for the UAV flight measurements during the period March 2017–March 2019, (A) the amount of manure present on the farm on the individual campaign days, (B) $CH_4$ emission factors of enteric fermentation and manure onsite.

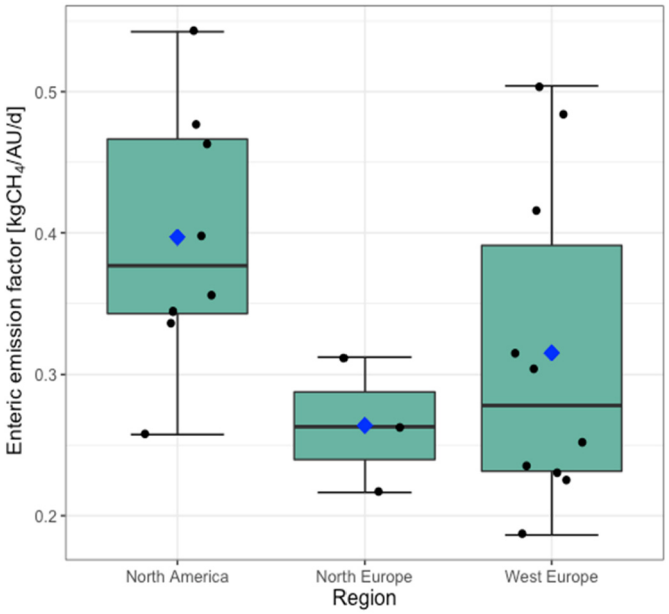


**Fig. 7.** Distribution of enteric emission factors based on the study region presented in Table 3. The whiskers indicate a minimum and maximum value, the black horizontal line inside the boxplot indicates the median value, the size of the box indicates 25–75 percentile, while the blue diamond presents a mean value. The black circles are enteric emission factors of each individual quantification.

four driving transects (Fig. 8b). During the UAV flight, the wind conditions became unstable making the choice of the sampling location with the UAV-based active AirCore system difficult, as the chance of missing the center of the plume would be higher, which may contribute to the slight underestimation of the mass balance approach. However, given the large uncertainties of both the MBA and IGA, the differences between the estimates and the actual release rate are not significant. Nevertheless, we have used the known $N_2O$ tracer release rate to derive a correction factor of 1.22 for the mass balance approach and 1.04 for the inverse Gaussian approach, respectively (Fig. 8a). With this $N_2O$-based correction applied to the derived $CH_4$ source strength, the agreement between the estimates from two UAV flights on 29 March 2019 has improved to be within ~0.2%, which has also reduced the 1-$\sigma$ variability of all five UAV-based MBA quantifications by ~17%, while the 1-$\sigma$ variability of ~10% two transects of van-based IGA quantifications decreased by ~5%.

Due to atmospheric variability, it is challenging to design appropriate flight heights, transect lengths, vertical spacings of transects, which must be chosen according to atmospheric dispersion parameters, i.e. the atmospheric stability (Andersen et al., 2021). In this study, mobile van measurements have been shown to be a good indicator of the plume location for the UAV-based active AirCore observations, since they cover a long driving path while transecting the plume downwind of the farm. Given that the dimensions of animal barns are comparable to the distances between the downwind transects (both the UAV and the mobile van) and the barns, the farm cannot be regarded as a point source but rather a line source or as a grid of point sources. Therefore, the transects should be long enough to cover the dispersed emissions, which adds complexity to the flight planning as the AirCore UAV flight time is limited to 7–13 min. To this end, in situ analysers deployed on UAVs will have advantages, provided that the precision and the accuracy are sufficiently high (Tuzson et al., 2020). On the other hand, the UAV-based AirCore system is capable of measuring multiple species, both $CH_4$ and a tracer $N_2O$, as demonstrated in this study, which provides a powerful tool of combining UAV-based mass balance quantification and a tracer release to accurately quantify $CH_4$ and potentially other greenhouse gases and air pollutants emissions. The UAV-based active AirCore system due to its flexibility and its mobility can obtain information that a van cannot, and at the same time, a van can measure multiple sources on a single day or record detailed temporal variation of a single source. Thus, mobile van measurements are a good but cumbersome indicator of the plume location for the UAV-based active AirCore observations. However, at this moment, there are no good cheap $CH_4$ sensors available on the market that could be used as a possible indicator of the plume location, except for a lightweight in situ airborne analyser that could be used as an indicator and analyser concurrently (Morales et al., 2021).

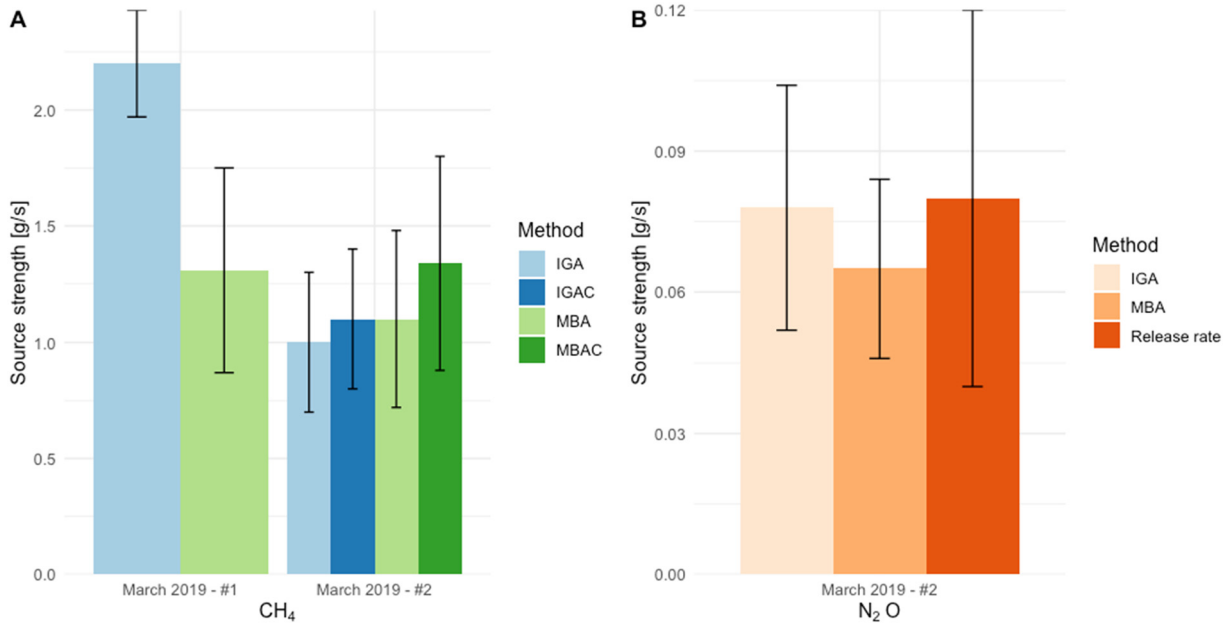


**Fig. 8.** The estimated source strength of the farm methane emission (a) and the estimated emission rate of the $N_2O$ tracer release (b), using the UAV based mass balance approach (MBA) and the van based inverse Gaussian approach (IGA), during a controlled $N_2O$ tracer release experiment on 29 March 2019. The MBAC presents a mass balance estimated source strength corrected based upon the $N_2O$ release rate, and IGAC a corrected Gaussian plume estimated source strength. The error bars indicate the uncertainty of each estimate for MBA, and IGA, respectively.

**Table 3**
A summary of estimated $CH_4$ emission factors from enteric fermentation based on farm-scale studies, along with the number of cows (including both lactating and dry), heifers, and calves, the average weight of cows, and the method used to quantify the emissions.

| Study | Number [head] | | Average weight of cows [kg] | Study region | Method | Enteric emission factor [kg $CH_4$ $AU^{-1}$ $d^{-1}$][a] |
|---|---|---|---|---|---|---|
| | Cows | Heifers/calves | | | | |
| VanderZaag et al. (2014) | | | | North America | | |
| Dairy 1 | 75 | 67 | 700 | | Open path $CH_4$ & IDM[c] | 0.26 |
| Dairy 2 | 113 | 108 | 750 | | Open path $CH_4$ & IDM | 0.35 |
| Arndt et al. (2018) | | | | | | |
| Dairy 1 | 3244 | 2793 | 454 | | Open path $CH_4$ & IDM | 0.34–0.40 |
| Dairy 2 | 2416 | 825 | 454 | | Open path $CH_4$ & IDM | 0.36–0.46 |
| Daube et al. (2019) | | | | | | |
| Dairy 1 | 3244 | 2793 | 454 | | Tracer plane | 0.48 |
| Dairy 2 | 2416 | 825 | 454 | | Tracer plane | 0.54 |
| | 164–195 | 0–10 | 600 | North Europe | VR*($CH_{4in}$-$CH_{4out}$) | 0.22–0.31 |
| Ngwabie et al. (2011) | 108 | – | 600 | | VR*($CH_{4in}$-$CH_{4out}$) | 0.17–0.36 |
| Jungbluth et al. (2001) | 55 | 20 | – | West Europe | [b]VR*($CH_{4in}$-$CH_{4out}$) | 0.20–0.25 |
| Fiedler and Müller (2011) | | | | | | |
| Dairy 1 | 364 | – | – | | VR*($CH_{4in}$-$CH_{4out}$) | 0.50 |
| Dairy 2 | 215 | – | – | | VR*($CH_{4in}$-$CH_{4out}$) | 0.24 |
| Saha et al. (2014) | 338–375 | – | 650–690 | | VR*($CH_{4in}$-$CH_{4out}$) | 0.25–0.32 |
| This study | 280 | 140 | 650 | | UAV $CH_4$ & MBA[d] | 0.20–0.51 |

[a] AU = Animal Unit (500 kg); the number of AU is calculated based on the number of lactating cows, dry cows, heifers, calves and the average weight of cows.
[b] VR = Ventilation Rate.
[c] IDM = Inverse Disperse Modeling.
[d] MBA = Mass Balance Approach.

## 4. Conclusions

In this study, we have estimated the $CH_4$ emissions from a dairy cow farm in the Netherlands on four individual days during the period from March 2017 to March 2019. Accurate atmospheric measurements of $CH_4$ mole fractions downwind of the farm were obtained using a UAV-based active AirCore system, once linked to accurate localized measurements of wind speed and direction. In addition, a $N_2O$ tracer release experiment at the farm was performed when both a UAV and a mobile van were used to simultaneously sample the $N_2O$ tracer and the $CH_4$ plumes from the farm.

The total $CH_4$ emission rates from the farm determined using the UAV-based mass balance approach ranged from 1.1–2.4 g/s, with an average emission rate of 1.7 ± 0.6 g/s over all quantifications. Its total uncertainty was dominated by the horizontal wind speed uncertainty and the uncertainty of the angle $\overline{\theta}$, and has been significantly improved with onsite continuous wind measurements from anemometers in more recent flights. Furthermore, we derived the enteric emission factors of 0.20–0.51 $kgCH_4/AU/d$ of dairy cows based on estimated emission rates from the mass balance approach and estimated emission factors of manure onsite, with the average $CH_4$ emission rate from enteric fermentation of 0.34 ± 0.13 $kgCH_4/AU/d$.

A $N_2O$ tracer release experiment showed that both the mass balance approach and the inverse Gaussian plume could retrieve the known $N_2O$ release rate within their uncertainties. However, the $N_2O$ tracer release experiment was performed only for a few hours and was certainly lacking of statistics. More simultaneous measurements between the UAV-based active AirCore system and a mobile van during a tracer release experiment are desired to better understand the uncertainties, and improve the accuracy, of both approaches. A slight disadvantage of the UAV AirCore approach is its relatively short-term observations (7–13 min) and that no real time $CH_4$ mole fraction measurements can be obtained during flights. Nevertheless, we have shown that mobile van measurements may be a good indicator of the plume location for the UAV-based active AirCore observations, and that the UAV-based AirCore system is capable of measuring both $CH_4$ and a tracer $N_2O$, suitable to be used to combine UAV-based mass balance approach and a tracer approach. The two mobile platforms, a van and a UAV, combined with the tracer approach can be a powerful tool to accurately quantify $CH_4$ emissions from a dairy cow farm and beyond.

## Declaration of competing interest

The authors declare that they have no known competing financial interests or personal relationships that could have appeared to influence the work reported in this paper.

## Acknowledgements

This research project is funded by the MEthane goes Mobile: MEasurement and Modeling (MEMO2) project from the European Union's Horizon 2020 research and innovation programme under the Marie Sklodowska-Curie grant agreement No 722479. The field measurements have been partially supported by funding from the European Research Council (ERC) under the European Union's Horizon 2020 research and innovation program under grant agreement No 742798 (http://cos-ocs.eu). We would like to thank Toine Cornelissen for his help with flying the drone during the campaigns, and we are very grateful to Roland Kooiker who has consistently supported our measurements near the farm over the past years.

## Appendix A. Supplementary data

Supplementary data to this article can be found online at https://doi.org/10.1016/j.scitotenv.2022.154898.

## References

Allen, G., Hollingsworth, P., Kabbabe, K., Pitt, J.R., Mead, M.I., Illingworth, S., Percival, C.J., 2018. The Development and Trial of an Unmanned Aerial System for the Measurement of Methane flux From Landfill and Greenhouse Gas Emission Hotspots.

Amon, B., Amon, T., Boxberger, J., Alt, C., 2001. Emissions of NH 3 , N 2 O and CH 4 From Dairy Cows Housed in a Farmyard Manure Tying Stall (Housing, Manure Storage, Manure Spreading), pp. 103–113.

Andersen, T., Scheeren, B., Peters, W., Chen, H., 2018. A UAV-based active AirCore system for measurements of greenhouse gases. Atmos. Meas. Tech. 11 (5), 2683–2699. https://doi.org/10.5194/amt-11-2683-2018.

Andersen, T., Vinkovic, K., de Vries, M., Kers, B., Necki, J., Swolkien, J., Chen, H., 2021. Quantifying methane emissions from coal mining ventilation shafts using an unmanned aerial vehicle (UAV)-based active AirCore system. Atmos. Environ. X 12 (May), 100135. https://doi.org/10.1016/j.aeaoa.2021.100135.

Arndt, C., Leytem, A.B., Hristov, A.N., Zavala-Araiza, D., Cativiela, J.P., Conley, S., Herndon, S.C., 2018. Short-term methane emissions from 2 dairy farms in California estimated by different measurement techniques and US Environmental Protection Agency inventory methodology: a case study. J. Dairy Sci. 101 (12), 11461–11479. https://doi.org/10.3168/jds.2017-13881.

Bernier, J.N., Undi, M., Plaizier, J.C., Wittenberg, K.M., Donohoe, G.R., Ominski, K.H., 2012. Impact of prolonged cold exposure on dry matter intake and enteric methane emissions of beef cows overwintered on low-quality forage diets with and without supplemented wheat and corn dried distillers' grain with solubles. Can. J. Anim. Sci. 92 (4), 493–500. https://doi.org/10.4141/CJAS2012-040.

Caulton, D.R., Li, Q., Bou-zeid, E., Fitts, J.P., Golston, L.M., Pan, D., Zondlo, M.A., 2018. Quantifying Uncertainties From Mobile-laboratory-derived Emissions of Well Pads Using Inverse Gaussian Methods, pp. 15145–15168.

Coenen, P.W.H.G., Van Der Maas, C.W.M., Zijlema, P.J., Arets, E.J.M.M., Baas, K., Van Den Berghe, A.C.W.M., te Biesebeek, J.D., Nijkamp, M.M., van Huis, E.P., Geilenkirchen, G., Versluijs, C.W., te Molder, R., Dröge, R., Montfoort, J.A., Peek, C.J., Vonk, J., 2014. Greenhouse gas emissions in The Netherlands 1990-2012. National Inventory Report 2014, National Institute for Public Health and the Environment (RIVM) Report 680355016/2014 . https://www.rivm.nl/publicaties/greenhouse-gas-emissions-in-netherlands-1990-2012-national-inventory-report-2014.

Daube, C., Conley, S., Faloona, I.C., Arndt, C., Yacovitch, T.I., Roscioli, J.R., Herndon, S.C., 2019. Using the tracer flux ratio method with flight measurements to estimate dairy farm CH4 emissions in Central California. Atmos. Meas. Tech. 12 (4), 2085–2095. https://doi.org/10.5194/amt-12-2085-2019.

Fiedler, A.M., Müller, H.J., 2011. Emissions of ammonia and methane from a livestock building natural cross ventilation. Meteorol. Z. 20 (1), 59–65. https://doi.org/10.1127/0941-2948/2011/0490.

Gao, Z., Yuan, H., Ma, W., Li, J., Liu, X., Desjardins, R.L., 2011. Diurnal and seasonal patterns of methane emissions from a dairy operation in North China plain. Adv. Meteorol. 2011, 7. https://doi.org/10.1155/2011/190234.

Grainger, C., Clarke, T., McGinn, S.M., Auldist, M.J., Beauchemin, K.A., Hannah, M.C., Eckard, R.J., 2007. Methane emissions from dairy cows measured using the sulfur hexafluoride (SF6) tracer and chamber techniques. J. Dairy Sci. 90 (6), 2755–2766. https://doi.org/10.3168/jds.2006-697.

Hanna, S.R., 1981. Handbook on Atmospheric Diffusion Models. 11223.

Hegarty, R.S., 2013. Applicability of short-term emission measurements for on-farm quantification of enteric methane. Animal 7 (Suppl. 2), 401–408. https://doi.org/10.1017/S1751731113000839.

Hensen, A., 2011. Methods for Observation and Quantification of Trace Gas Emissions From Diffuse Source. Vrije Universiteit.

IPCC, 2006. Chapter 10: Emissions from livestock and manure managment. In: Eggleston, H.S., Buendia, L., Miwa, K., Ngara, T., Tanabe, K. (Eds.), 2006 IPCC Guidelines for National Greenhouse Gas Inventories, vol.4: Agriculture, Forestry and Other Land Use. IGES, Japan ISBN 4-88788-032-4.

IPCC, 2014. In: Field, C.B., Barros, V.R., Dokken, D.J., Mach, K.J., Mastrandrea, M.D., Bilir, T.E., Chatterjee, M., Ebi, K.L., Estrada, Y.O., Genova, R.C., Girma, B., Kissel, E.S., Levy, A.N., MacCracken, S., Mastrandrea, P.R., White, L.L. (Eds.), Climate Change 2014: Impacts, Adaptation, and Vulnerability. Part A: Global and Sectoral Aspects. Contribution of Workinh Group II to the Fifth Assessment Report of the Intergovernmental Panel on Climate Change. Cambridge University Press, Cambridge, United Kingdom and New York, NY, USA 1132 pp.

Joo, H.S., Ndegwa, P.M., Heber, A.J., Ni, J., Bogan, B.W., Ramirez-dorronsoro, J.C., Cortus, E., 2015. Greenhouse Gas Emissions From Naturally Ventilated Freestall Dairy Barns. 102, pp. 384–392. https://doi.org/10.1016/j.atmosenv.2014.11.067.

Jungbluth, T., Hartung, E., Brose, G., 2001. Greenhouse gas emissions from animal houses and manure stores. Nutr. Cycl. Agroecosyst. 60 (1–3), 133–145. https://doi.org/10.1023/A:1012621627268.

Moe, P.W., Tyrrell, H.F., 1979. Methane production in dairy cows. J. Dairy Sci. 62 (10), 1583–1586. https://doi.org/10.3168/jds.S0022-0302(79)83465-7.

Morales, R., Ravelid, J., Vinkovic, K., Korbe, P., Tuzson, B., Emmenegger, L., Chen, H., Schmidt, M., Humbel, S., Brunner, D., 2021. A Tracer Release Experiment to Investigate Uncertainties in Drone-based Emission Quantification for Methane Point Sources. November, pp. 1–34. https://doi.org/10.5194/amt-2021-314.

Myers, D.E., 1991. Interpolation and estimation with spatially located data. W Tutorial 209 Chemometrics and Intelligent Laboratory Sysiems. 11.

Myhre, G., Shindell, D., Bréon, F.-M., Collins, W., Fuglestvedt, J., Huang, J., Koch, D., Lamarque, J.-F., Lee, D., Mendoza, B., Nakajima, T., Robock, A., Stephens, G., Takemura, T., Zhang, H., 2013. Anthropogenic and natural radiative forc- ing. In: Stocker, T.F., Qin, D., Plattner, G.-K., Tignor, M., Allen, S.K., Boschung, J., Nauels, A., Xia, Y., Bex, V., Midgley, P.M. (Eds.), Climate Change 2013: The Physical Science Basis. Contribution of Working Group I to the Fifth Assessment Report of the Intergovernmental Panel on Climate Change. Cambridge University Press, Cambridge, United Kingdom and New York, NY, USA.

Nathan, B.J., Golston, L.M., O'Brien, A.S., Ross, K., Harrison, W.A., Tao, L., Zondlo, M.A., 2015. Near-field characterization of methane emission variability from a Compressor Station using a model aircraft. Environ. Sci. Technol. 49 (13), 7896–7903. https://doi.org/10.1021/acs.est.5b00705.

Ngwabie, N.M., Jeppsson, K.H., Gustafsson, G., Nimmermark, S., 2011. Effects of animal activity and air temperature on methane and ammonia emissions from a naturally ventilated building for dairy cows. Atmos. Environ. 45 (37), 6760–6768. https://doi.org/10.1016/j.atmosenv.2011.08.027.

Ngwabie, N.M., Jeppsson, K.H., Nimmermark, S., Swensson, C., Gustafsson, G., 2009. Multi-location measurements of greenhouse gases and emission rates of methane and ammonia from a naturally-ventilated barn for dairy cows. Biosyst. Eng. 103 (1), 68–77. https://doi.org/10.1016/j.biosystemseng.2009.02.004.

Ngwabie, Ngwa M., Vanderzaag, A., Jayasundara, S., Wagner-Riddle, C., 2014. Measurements of emission factors from a naturally ventilated commercial barn for dairy cows in a cold climate. Biosyst. Eng. 127, 103–114. https://doi.org/10.1016/j.biosystemseng.2014.08.016.

Nisbet, E.G., Manning, M.R., Dlugokencky, E.J., Fisher, R.E., Lowry, D., Michel, S.E., White, J.W.C., 2019. Very strong atmospheric methane growth in the 4 years 2014–2017: implications for the Paris agreement. Glob. Biogeochem. Cycles 33 (3), 318–342. https://doi.org/10.1029/2018GB006009.

Ruyssenaars, P.G., Coenen, P.W.H.G., Rienstra, J.D., Zijlema, P.J., Arets, E.J.M.M., Baas, K., Dröge, R., Geilenkirchen, G., Honig, B., van Huet, B., van Huis, E.P., Koch, W.W.R., te Molder, R.M., Montfoort, J.A., van der Zee, T., van Zanten, M.C., t'Hoen, M., 2019. Greenhouse gas emissions in The Netherlands 1990-2019. National Inventory Report 2019. National Institute for Public Health and the Environment (RIVM) https://doi.org/10.21945/RIVM-2021-0007. https://rivm.openrepository.com/handle/10029/624862.

Ruyssenaars, P.G., Coenen, P.W.H.G., Rienstra, J.D., Zijlema, P.J., Arets, E.J.M.M., Baas, K., Dröge, R., Geilenkirchen, G., 't Hoen, M., Honig, E., van Huet, B., van Huis, E.P., Koch, W.W.R., te Molder, R.M., Montfoort, J.A., van der Zee, T., van Zanten, M.C., 2021. Greenhouse gas emissions in the Netherlands 1990-2019. National Inventory Report 2021. National Institute for Public Health and the Environment (RIVM), RIVM-2021-0007. https://www.rivm.nl/bibliotheek/rapporten/2021-0007.pdf.

Saha, C.K., Ammon, C., Berg, W., Fiedler, M., Loebsin, C., Sanftleben, P., Amon, T., 2014. Seasonal and diel variations of ammonia and methane emissions from a naturally ventilated dairy building and the associated factors influencing emissions. Sci. Total Environ. 468–469, 53–62. https://doi.org/10.1016/j.scitotenv.2013.08.015.

Saunois, M., Bousquet, P., Poulter, B., Peregon, A., Ciais, P., Canadell, J.G., Zhu, Q., 2016. The global methane budget 2000–2012. Earth Syst. Sci. Data 8 (2), 697–751. https://doi.org/10.5194/essd-8-697-2016.

Shah, A., Pitt, J.R., Ricketts, H., Leen, J.B., Williams, P.I., Kabbabe, K., Gallagher, M.W., Allen, G., 2020. Testing the near-field Gaussian plume inversion flux quantification technique using unmanned aerial vehicle sampling. Atmos. Meas. Tech. 13, 1467–1484. https://doi.org/10.5194/amt-13-1467-2020.

Tuzson, B., Graf, M., Ravelid, J., Scheidegger, P., Kupferschmid, A., Looser, H., Morales, R.P., Emmenegger, L., 2020. A compact QCL spectrometer for mobile, high-precision methane sensing aboard drones. Atmos. Meas. Tech. 13, 4715–4726. https://doi.org/10.5194/amt-13-4715-2020.

VanderZaag, A.C., Flesch, T.K., Desjardins, R.L., Baldé, H., Wright, T., 2014. Measuring methane emissions from two dairy farms: seasonal and manure-management effects. Agric. For. Meteorol. 194, 259–267. https://doi.org/10.1016/j.agrformet.2014.02.003.

Wu, W., Zhang, G., Kai, P., 2012. Ammonia and methane emissions from two naturally ventilated dairy cattle buildings and the influence of climatic factors on ammonia emissions. Atmos. Environ. 61, 232–243. https://doi.org/10.1016/j.atmosenv.2012.07.050.

Zhang, G., Strøm, J.S., Li, B., Rom, H.B., Morsing, S., Dahl, P., Wang, C., 2005. Emission of ammonia and other contaminant gases from naturally ventilated dairy cattle. Buildings 92, 355–364. https://doi.org/10.1016/j.biosystemseng.2005.08.002.